



Dynamic Response of Submerged Vertical Cylinder with Lumped Mass under Seismic Excitation

M. Shahmardani^a, J. Mirzapour^{*a}, S. Tariverdilo^b

^a Department of Civil and Environmental Engineering, Politecnico di Milano, Milan, Italy

^b Department of Civil Engineering, Urmia University, Urmia, Iran

PAPER INFO

Paper history:

Received 10 January 2014

Received in revised form 15 June 2014

Accepted 26 June 2014

Keywords:

Vertical Circular Cylinder

Seismic Excitation

Lumped Mass

Added Mass

ABSTRACT

An analytical approach is presented to assess the response of offshore structures under seismic excitation. This paper evaluates the impacts of different fluid field models and the mass of equipment at the top of offshore structure which is simulated as lumped mass on the responses of offshore structures. To do this, two and three dimensional fluid field models are developed. In three dimensional models different approximation regarding the free surface boundary condition associated with high and low frequency excitations are adopted. Then the alternation of response of structure with changing in the value of lumped mass is calculated. Finally the impacts of different models on the value of maximum displacement for Kobe earthquake are evaluated. It is shown that different approximations regarding the fluid field could largely change the value of maximum displacement evaluated by the models.

doi: 10.5829/idosi.ije.2014.27.10a.08

1. INTRODUCTION

For maximum water depth less than 1000 m, it is usual to use platforms fixed in the bottom. Fixed bottom platforms include different kinds ranging from jackup rigs, gravity platforms, jacket platforms to compliant tower platforms. Considering fixed platforms, equipment mass is simulated as lumped mass at the top of offshore structure. The surrounding fluid could have large impact on overall response of these structures when they are excited by earthquakes. The mathematical derivation of fluid-structure interaction requires some approximation on the fluid field that could affect the magnitude of the response estimated by the model.

Yeung [1] found the added mass and damping of floating circular cylinder in finite depth water. He derived added mass and damping for heave, sway and roll motions of the cylinder. Rahman et al. [2] obtained

added mass and damping coefficients for a circular cylinder clamped at the seabed. They used eigenfunction expansion including propagating and evanescent modes and finally developed asymptotic high and low frequency solutions for added mass and added damping. Williams [3] investigated dynamic response of surface piercing clamped circular cylinder under horizontal ground excitation. Employing high frequency approximation of free surface boundary condition, he developed Green function to obtain integral solution for compressible fluid flow. Tung [4] studied the behavior of submerged vertical cylindrical tank under harmonic ground excitations. Assuming incompressible, inviscid and irrotational fluid flow, Laplace equation was solved for two inner and outer regions of the fluid field and then, applying boundary and continuity conditions, hydrodynamic forces were obtained and effect of tank geometry properties on the hydrodynamic forces in graphical form were presented. Maheri et al. [5] experimentally calculated the added mass for rigid and flexible cylinders. Han et al. [6] derived an analytical solution for added mass of flexible cylinder under harmonic ground motion

*Corresponding Author's Email: Mirzapour.jamil@gmail.com (J. Mirzapour)

excitation. They also developed a simple formula for computing natural frequency of the coupled system. Hsi-teh [7] investigated earthquake response of circular column for partially submerged water. The added mass for submerged floating tunnel in the case of deep and shallow water was derived by Shahmardani et al. [8].

Anagnostopoulos [9] who studied dynamic response of offshore platforms under wave loading used a time domain solution using Morrison's equation to account for fluid-structure interaction. Lee et al. [10] investigated the seismic response of flexible underwater oil storage tanks under horizontal ground motion. Bhata et al. [11] investigated dynamic response of vertical circular cylinder under wave loads with small amplitude. They considered three motions, surge, heave and pitch in finite-depth water and assuming four velocity potentials for water field, utilized an analytical solution for solution of fluid-structure interaction. Wu et al. [12] obtained exact solutions for natural frequencies and mode shapes of an immersed wedge beam with a tip mass at the end. They found good agreement between their results and finite element method. Oz [13] used analytical and finite element methods to calculate natural frequency of a beam partially immersed in the water with a tip mass. He considered transverse vibration of beam and showed that by increase in water height, tip mass and water density, there is a decrease in natural vibration frequencies. Naghipour [14] described various time-domain methods useful for analyzing the experimental data obtained from a circular cylinder force in terms of both wave and current for estimation of the drag and inertia coefficients applicable to the Morrison's equation.

Esper [15] investigated the seismic response of an offshore structure using ANSYS. He used Westergaard added mass model to account for fluid structure interaction. He concluded that accounting for inertial effect of surrounding water reduces the maximum acceleration at platform level. Amundsen [16] investigated the influence of different models regarding fluid-structure interaction on the overall seismic response of a concrete platform. He considered two models, the first is an added mass model employing Morrison's equation and the second involves coupled analysis of the fluid and structure fields in ABAQUS. He found that although the change in the period of the system in the two models is negligible, the frequency content of the responses could have appreciable differences. The effect of added mass fluctuation on vertical vibration of TLP in the case of vibration in still water for both free and forced vibration subjected to axial load at the top of the leg was presented by Tabeshpour et al. [17].

Accounting for fluid-structure interaction through a complex coupled field analyses is numerically expansive. On the other hand, oversimplification of

this interaction through commonly adopted Morrison's equation, which does not account for reduced added mass near free surface, could significantly affect the accuracy of the analysis. This shows the need for analytical models capable of reproducing global response of the coupled field with good accuracy.

In this study, dynamic response of vertical circular cylinder with lumped mass is investigated under seismic excitation. Two and three dimensional models are adopted to consider fluid-structure interaction. Then governing equation of the system under simultaneous application of the fluid pressure and seismic excitation is obtained. Finally, variations of maximum displacement and natural frequencies of the coupled system with change in the ratio of lumped mass to the cylinder mass are investigated.

2. FORMULATION FOR JACKET

Offshore structure is simulated as a vertical circular cylinder with a lumped mass which is the mass of equipment at the top of it. As it has been shown in Figure 1, height, radius and thickness of cylinder are denoted by h , r and t , respectively; and lumped mass M is located at the top of cylinder. In this study the only rotary inertia of the lumped mass is ignored. The equilibrium equation of the cylinder with surrounding water is (Williams and Moubayed [18]):

$$m \frac{\partial^2 w_t}{\partial t^2} + EI \frac{\partial^4 w}{\partial z^4} = m \ddot{w}_t + EI w^{(iv)} = F \quad (1)$$

where m and EI are mass per unit length of cylinder and flexural rigidity of cylinder. Decomposing the deflection of the cylinder we have:

$$w_t(z, t) = w(z, t) + w_g(g) \quad (2)$$

here w and w_g are total and relative (to ground) lateral deflection of cylinder and w_g is ground displacement. In Equation 1, F simulates the external fluid force on cylinder body. The boundary conditions of cylinder are (To [19]):

$$\begin{aligned} w|_{z=0} &= 0 \\ \frac{\partial w}{\partial z}|_{z=0} &= 0 \\ EI \frac{\partial^2 w}{\partial z^2}|_{z=h} &= 0 \\ EI \frac{\partial^3 w}{\partial z^3}|_{z=h} &= M \frac{\partial^2 w}{\partial t^2}|_{z=h} \end{aligned} \quad (3)$$

Considering free vibration of beam ($F=0$ in Equation 1) with tip mass (boundary conditions of Equation 3), we could derive the eigen-functions (mode shapes) of

the beam. Now, employing Equation (2), we could expand total lateral deflection in terms of eigenfunctions of beam with tip mass as [19]:

$$w_t(z, t) = \sum_{n=1}^{\infty} A_n(t) \left[\sinh \varepsilon_n \frac{z}{h} - \sin \varepsilon_n \frac{z}{h} - \frac{\sin \varepsilon_n + \sinh \varepsilon_n}{\cos \varepsilon_n + \cosh \varepsilon_n} \left(\cosh \varepsilon_n \frac{z}{h} - \cos \varepsilon_n \frac{z}{h} \right) \right] \quad (4)$$

$$+ w_g(t) = \sum_{n=1}^{\infty} A_n(t) \phi_n(z) + w_g(t)$$

where $A_n(t)$ is modal amplitude of the n^{th} mode and ε_n is corresponding eigen-value. The eigen-value is determined solving the following equation [19]:

$$\varepsilon_n \frac{\sin \varepsilon_n \cosh \varepsilon_n - \sinh \varepsilon_n \cos \varepsilon_n}{1 + \cos \varepsilon_n \cosh \varepsilon_n} = \frac{mh}{M} = \frac{1}{\alpha} \quad (5)$$

Hereafter we define α as mass ratio. As it is shown in Figure 2, increasing the ratio of lumped mass to mass per length of cylinder (M/mh or mass ratio) there is decrease in the value of ε_n , which these decreases are smaller for higher mode numbers. On the other hand, as it could be inferred from this figure, for larger mass ratios the change in the value of eigenvalue decreases and they become essentially constant.

3. FORMULATION FOR FLUID FIELD

Accounting for fluid-structure interaction through a complex coupled field analyses is numerically expansive. On the other hand, oversimplification of this interaction through commonly adopted Morrison's equation does not account for reduced added mass near free surface and consequently could affect the accuracy of the analysis. This shows the need for numerical inexpensive analytical models capable of reproducing global response of the coupled field with good accuracy. Assuming that the surrounding fluid is incompressible, inviscid and for irrotational fluid flow, it is possible to treat the flow field by potential theory. With this assumptions, the velocity potential function should satisfy Laplace equation:

$$\nabla^2 \phi = 0 \quad (6)$$

Here we adopt two approaches to evaluate the fluid pressure on the cylinder body. In the first approach, the fluid field is treated as two dimensional (2D) field, assuming constant inertial effect of the fluid field along cylinder length (ignoring free surface boundary condition). In the second approach, the fluid field is treated as three dimensional (3D) field to account for the change in the inertial contribution of the fluid field along the cylinder length (especially near free surface).

The 3D models are developed employing simplification of free surface boundary condition. Two 3D models are developed which are only applicable for

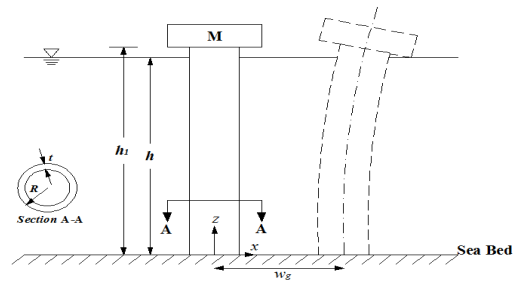


Figure 1. Schematic view of vertical circular cylinder

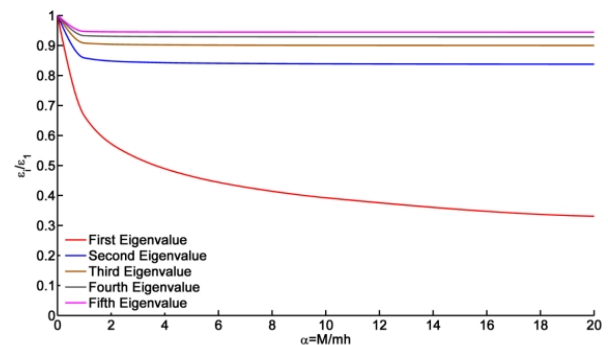


Figure 2. Variations of eigenvalues with changing in the mass ratio

excitation with high or low frequency content. These analytical models could provide an upper and lower boundaries for displacement of the offshore. The general free surface boundary condition has the following form:

$$\frac{\partial^2 \phi}{\partial t^2} + g \frac{\partial \phi}{\partial z} = 0 \quad (7)$$

To derive the simplified free surface boundary condition for high and low frequency excitation, we consider harmonic excitation in the form of $e^{i\omega t}$. For this excitation we have:

$$\phi(r, \theta, z, t) = e^{i\omega t} \phi(r, \theta, z) \quad (8)$$

now the boundary condition (7) becomes:

$$\frac{\partial^2 \phi}{\partial t^2} + g \frac{\partial \phi}{\partial z} = (-\omega^2 \phi(r, \theta, z) + g \frac{\partial \phi(r, \theta, z)}{\partial z}) e^{i\omega t} \quad (9)$$

and consequently:

$$-\omega^2 \phi_1(r, \theta, z) + g \frac{\partial \phi(r, \theta, z)}{\partial z} = 0 \quad (10)$$

Considering low frequency excitation, this leads to:

$$\frac{\partial \phi(r, \theta, z)}{\partial z} = 0 \quad (11)$$

and for high frequency excitation to:

$$\varphi(r, \theta, z) = 0 \quad (12)$$

In the following subsections, the solutions for two and three dimensional fluid fields are presented.

3. 1. Two Dimensional Fluid Field For two dimensional case, the Laplace Equation (6) becomes:

$$\nabla^2 \varphi = \frac{\partial^2 \varphi}{\partial r^2} + \frac{1}{r} \frac{\partial \varphi}{\partial r} + \frac{1}{r^2} \frac{\partial^2 \varphi}{\partial \theta^2} = 0 \quad (13)$$

$$R \leq r, \quad 0 \leq \theta \leq 2\pi$$

The potential function must also satisfy the following boundary conditions:

$$\lim_{r \rightarrow \infty} \varphi = 0 \quad (14)$$

$$\left. \frac{\partial \varphi}{\partial r} \right|_{r=R} = \dot{w}_t \cos \theta$$

The first boundary condition accounts for still water in large distance from the jacket, and the second boundary condition satisfies the compatibility of deflection in the fluid-structure interface. Imposing the boundary conditions, the velocity potential function is obtained in the following form:

$$\varphi(r, \theta) = -\dot{w}_t \frac{R^2}{r} \cos \theta \quad (15)$$

Integrating the fluid pressure on wet surface of the cylinder, the fluid force will be:

$$F = -\rho_f \pi R^2 \ddot{w}_t = -m_a \ddot{w}_t \quad (16)$$

Now introducing this fluid force in Equation (1), we have:

$$(m + m_a) \ddot{w}_t + EI w^{(iv)} = 0 \quad (17)$$

Substituting w_t from Equation (4), multiplying both sides of equation by φ_i and integrating through the length of the beam and finally employing the orthogonality of cylinder's mode shapes, the differential equation for modal amplitudes could be derived:

$$(m + m_a) \ddot{A}_i + EI \varepsilon_i^4 A_i(t) = -\frac{2}{L} F_i \quad (18)$$

$$F_i = (m + m_a) \int_0^h \phi_i(z) \ddot{w}_g(t) dz$$

3. 2. Three Dimensional Fluid Field The three-dimensional model accounts for the change in the inertial contribution of the fluid along the cylinder length. In this section the external force is calculated for two different conditions, imposing different assumptions regarding the free surface boundary

condition. In this case the Laplace equation takes the following form:

$$\nabla^2 \varphi = \frac{\partial^2 \varphi}{\partial r^2} + \frac{1}{r} \frac{\partial \varphi}{\partial r} + \frac{1}{r^2} \frac{\partial^2 \varphi}{\partial \theta^2} + \frac{\partial^2 \varphi}{\partial z^2} = 0 \quad (19)$$

subjected to the following boundary conditions:

$$\varphi = 0 \quad \text{as } r \rightarrow \infty \quad (20a)$$

$$\left. \frac{\partial \varphi}{\partial r} \right|_{r=R} = \dot{w}_t \cos \theta \quad \text{at } r = R \quad (20b)$$

$$\left. \frac{\partial \varphi}{\partial z} \right|_{z=0} = 0 \quad \text{at } z = 0 \quad (20c)$$

The first equation accounts for still water at large distance from jacket, and the second equation considers the compatibility of deflection between jacket and its surrounding water. The last equation is the impermeability boundary condition at bottom (no fluid flow (velocity) in the direction normal to sea bed).

We derive the asymptotic solution for two cases of near zero and high frequency excitations. To do this, two 3D solution accounting for two simplified boundary conditions for free surface (Equations (11) and (12)) are considered.

Considering Equation (12), in the case of high frequency excitation (solution denoted by φ_1), the free surface boundary condition simplifies to:

$$\varphi_1 = 0 \quad \text{at } z = h \quad (21)$$

In the same time, considering Equation (11), for near zero (low) frequency excitation (solution denoted by φ_2), the free surface boundary condition reduces to:

$$\left. \frac{\partial \varphi_2}{\partial z} \right|_{z=h} = 0 \quad \text{at } z = h \quad (22)$$

Imposing the boundary conditions, the analytical solution for the potential function are obtained as:

$$\varphi_1(r, \theta, z, t) = \sum_{m=1}^{\infty} B_m(t) K_1(\lambda_m r) \cos(\lambda_m z) \cos \theta \quad (23)$$

$$\lambda_m = \frac{(2m-1)\pi}{2h}$$

and

$$\varphi_2(r, \theta, z, t) = \sum_{m=1}^{\infty} A_m(t) K_1(\beta_m r) \cos(\beta_m z) \cos \theta \quad (24)$$

$$\beta_m = \frac{m\pi}{h}$$

where K_1 is the modified Bessel function of second kind of order one and λ_m and β_m are the problem eigenvalues. The only difference between two solutions is in the value of eigenvalues. To avoid repetitive derivations, we only derive the solution for φ_1 .

Considering the compatibility condition at fluid-structure interface, we conclude:

$$\sum_{m=1}^{\infty} B_m(t) \lambda_m K'_1(\lambda_m R) \cos(\lambda_m z) \cos(\theta) \quad (25)$$

$$= \sum_{n=1}^{\infty} [\phi_n(z) A_n(t) + \dot{w}_g] \cos(\theta)$$

Now making use of the orthogonality of harmonic functions, we have:

$$B_i(t) = \frac{2}{h \lambda_i K'_1(\lambda_i R)} \sum_{n=1}^{\infty} [\gamma_{ni} A_n(t) + \gamma_i \dot{w}_g(t)] \quad (26)$$

where:

$$\gamma_{ni} = \int_0^h \cos(\lambda_i z) \phi_n(z) dz \quad (27)$$

$$\gamma_n = \int_0^h \cos(\lambda_i z) dz$$

Thus the potential function takes the following form:

$$\phi_1(r, \theta, z, t) = \sum_{m=1}^{\infty} \sum_{n=1}^{\infty} \frac{2 K_1(\lambda_m r)}{h \lambda_m K'_1(\lambda_m R)} [\gamma_{nm} \dot{A}_n + \gamma_m \dot{w}_g(t)] \cos(\lambda_m z) \cos(\theta) \quad (28)$$

Integrating the fluid pressure over the cylinder wet surface, the fluid induced inertial force imposed on the structure could be evaluated as:

$$F_1 = -m_a \sum_{m=1}^{\infty} \sum_{n=1}^{\infty} [\gamma_{nm} \ddot{A}_n + \gamma_m \ddot{w}_g(t)] C_m \cos(\lambda_m z) \quad (29)$$

where

$$C_m = \frac{2 K(\lambda_m R)}{h \lambda_m R K'_1(\lambda_m R)} \quad (30)$$

Introducing this fluid force in structure's equilibrium equation (Equation (1)), we have:

$$\sum_{m=1}^{\infty} EI \phi_m^{iv}(z) A_m(t) + m \sum_{m=1}^{\infty} \phi_m(z) \ddot{A}_m(t) + m \ddot{w}_g(t) + m_a \sum_{m=1}^{\infty} \sum_{n=1}^{\infty} [\gamma_{nm} \ddot{A}_n + \gamma_m \ddot{w}_g(t)] C_m \cos(\lambda_m z) = 0 \quad (31)$$

Multiplying both sides of Equation (31) by $\phi_i(z)$ and integrating over 0 to h , we obtain a set of coupled ordinary differential equations:

$$EI \left(\frac{\varepsilon_i}{h}\right)^4 A_i(t) + m \ddot{A}_i(t) + m_a \sum_{m=1}^{\infty} \sum_{n=1}^{\infty} C_m \gamma_{nm} \frac{\gamma_{im}}{D_{im}} \ddot{A}_n(t) = -\frac{F_{s1}}{D_{im}} \quad (32)$$

$$F_{s1} = \left[m_a \sum_{m=1}^{\infty} C_m \gamma_m \gamma_{im} + m E_i \right] \ddot{w}_g(t) = [M_{Fs1} + m E_i] \ddot{w}_g(t)$$

$$D_{im} = \int_0^h \phi_i \phi_m dz$$

$$E_i = \int_0^h \phi_i(z) dz$$

The differential equation for modal amplitudes of φ_2 becomes:

$$EI \left(\frac{\varepsilon_i}{h}\right)^4 B_i(t) + m \ddot{B}_i(t) + m_a \sum_{m=1}^{\infty} \sum_{n=1}^{\infty} C_m \gamma_{nm} \frac{\gamma_{im}}{D_{im}} \ddot{B}_n(t) = -\frac{F_{s2}}{D_{im}} \quad (32)$$

$$F_{s2} = \left[m_a \sum_{m=1}^{\infty} C_m \gamma_m \gamma_{im} + m E_i \right] \ddot{w}_g(t) = [M_{Fs2} + m E_i] \ddot{w}_g(t)$$

These sets of differential equations are solved using 4th order Runge-Kutta integration method. The added mass matrix will have following components:

$$m_{in} = m_a \sum_{m=1}^{\infty} C_m \gamma_{mi} \frac{\gamma_{im}}{D_{im}} \quad (34)$$

Existence of off-diagonal terms in this matrix shows the coupling of different modes in the differential equation for modal amplitudes.

In Equations (32) and (33), F_{s1} and F_{s2} represent the earthquake induced lateral force along the cylinder external surface. These forces are composed of two terms. The first term is due to fluid flow adjacent to the cylinder body and the second term is associated with the cylinder's own inertia. Note that difference in the value of F_{s1} and F_{s2} comes from the difference in the value of eigenvalues λ_m and β_m . Figure 3 depicts the variation of M_{Fs1} and M_{Fs2} (masses associated with F_{s1} and F_{s2}) with mass ratio and mode number. Interesting point is that while M_{Fs1} (the mass associated with the fluid induced lateral force on the cylinder body in the case of high frequency excitation) is larger for decreasing mode numbers and increasing mass ratios, M_{Fs2} (the mass associated with the fluid induced lateral force on the cylinder body in the case of low frequency excitation) becomes zero for all mass ratios and mode numbers. This shows that in the case of low frequency excitation, the lateral force along cylinder body comes only from the mass inertia of cylinder and there is no contribution from surrounding fluid.

Figure 4 shows the evolution of three dimensional added mass matrix for the cases of high and low frequency excitations when lumped mass is equal to zero. As it is evident from this figure, for both types of excitations diagonal terms are significantly larger than off-diagonal ones. This is an indication of negligible coupling between different modes in both cases.

Variations of diagonal terms of added mass matrix with changes in the mass ratio are shown in Figure 5. As it could be inferred from this figure, there is completely different pattern for low and high frequency excitations in the case of low mass ratios. For higher mass ratios in both cases diagonal terms of added mass matrix are insensitive to the change in the mass ratio.

Figure 6 illustrates a comparison of the diagonal terms of added mass matrix, obtained using two-dimensional and three-dimensional models. It is shown that while in the 2D model, the value of added mass remains constant for different modes, in the 3D model, different modes have different ratios of added mass

which are less than the 2D model. This reduction in the added mass of 3D model is due to imposition of impermeability and free surface boundary conditions in this model.

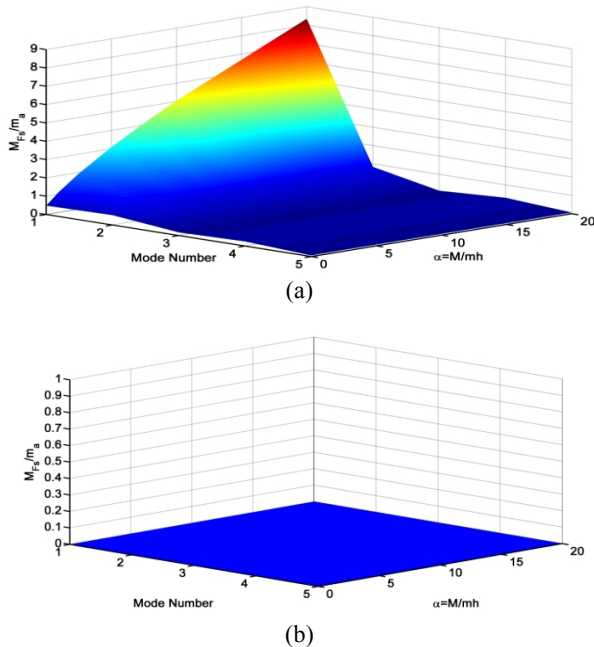


Figure 3. Variations of masses M_{Fs1} and M_{Fs2} with change in mass ratio and mode number, a) high frequency excitation and b) low frequency excitation

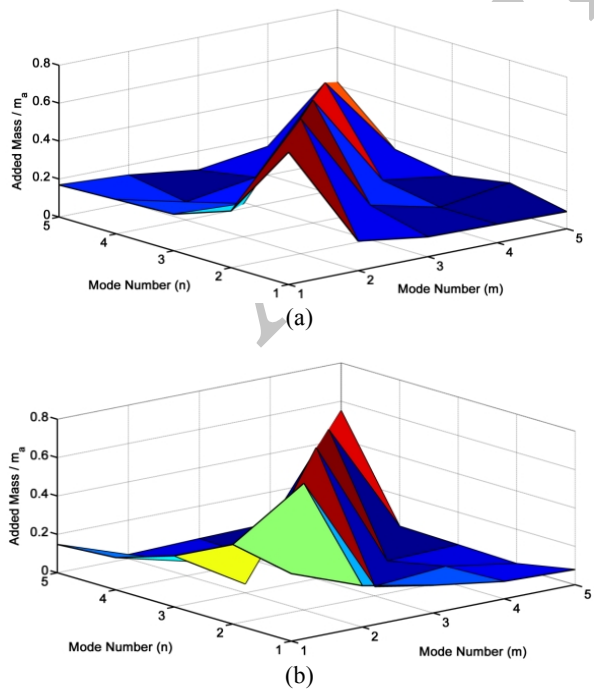


Figure 4. Value of different elements of added mass matrix for five modes in the case of zero lumped mass ($M=0$), a) high frequency excitation and b) low frequency excitation

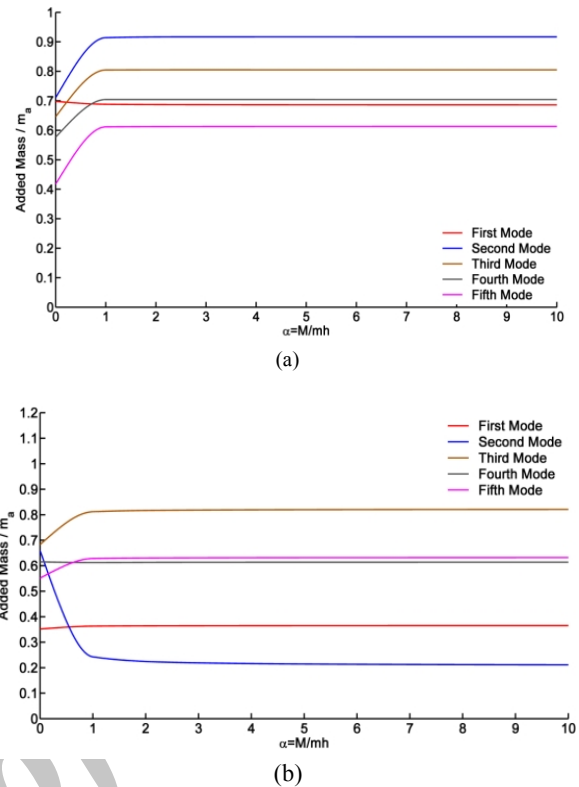


Figure 5. Evolution of diagonal terms of added mass matrix with mass ratio, a) high frequency excitation and b) low frequency excitation

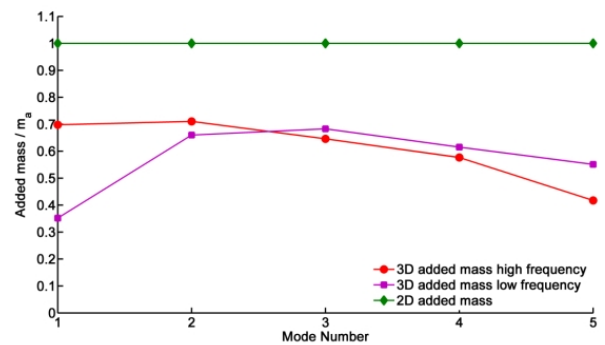
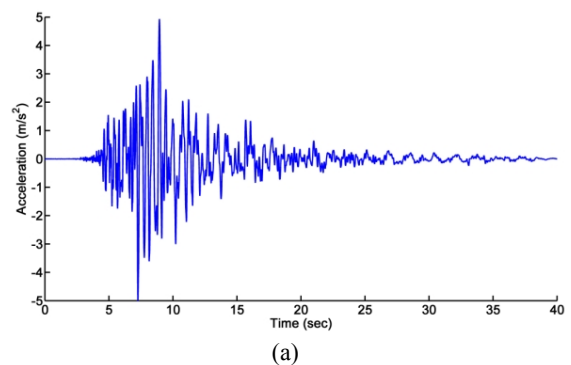


Figure 6. Comparison of diagonal terms of added mass matrixes in 2D and 3D models



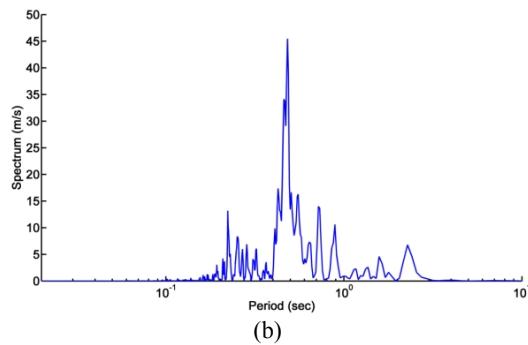


Figure 7. Kobe ground motion record, a) time history and b) Fourier decomposition.

4. GROUND MOTION EXCITATION

To evaluate the extent of the variation in response due to change in assumption regarding fluid field, in this section results of analysis of offshore structure for ground Kobe ground motion excitation are presented. The result shows how different models regarding fluid field could affect the evaluated response. By evaluating the response to Kobe ground motion record, it is not intended to obtain a global judgment about seismic response of the offshore structures. The main focus of the paper is on assessing the difference in the seismic response due to assumed models for fluid field.

Tabulated in Table 1 are the values of the parameters used in the analysis of reinforced concrete vertical cylinder. Analyses are done for ground motion record of Kobe earthquake (090 component of 1995 Kobe earthquake at Japan recorded at Nishi-Akashi station, KOBE/NIS000). In the following simulations the same value for h and h_1 is used. Table 2 shows duration, peak ground acceleration and epicentral distance of ground motion record. Figure 7 depicts time history of the ground motion record and its Fourier spectrum.

Figure 8 presents the variation in the natural frequencies of cylinder for different mass ratios for 3D model with high and low frequency excitations and 2D fluid field model, where ω_1 and ω_i are first natural frequency of cylinder when mass ratio is equal to zero ($\alpha=0$) and natural frequencies of cylinder for different added mass ratios, respectively. In all models the largest change in the frequency is for the first mode. For large mass ratios, which is applicable for most of platforms, 3D fluid model applicable for high frequency excitation results in lower frequencies in nearly all modes compared to the other models. This indicates that the participation of higher modes in 3D model applicable for higher frequencies could be higher compared to the other models and as expected this model could give better estimate of actual response for excitations rich in higher frequencies.

Evolution of maximum displacement at the top of structure with change in the mass ratio for four different cases, including 3D models with high and low frequency excitations, 2D model and ignoring fluid field (dry cylinder) are depicted in Figure 9. It can be seen that maximum displacement occurs when lumped mass is equal to zero and by increasing the value of lumped mass the maximum displacements decreases in all cases.

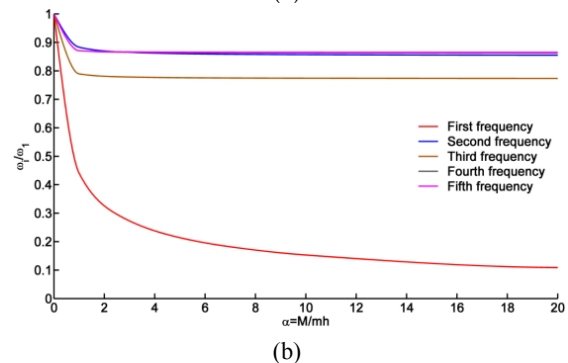
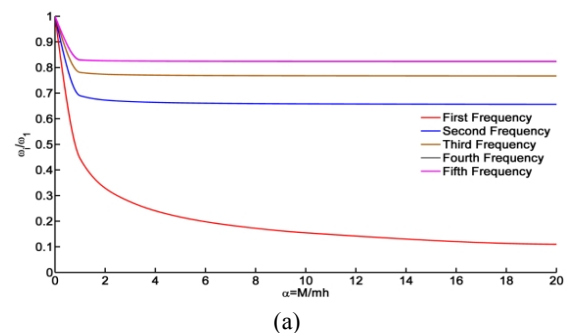
Interesting point is that maximum displacement in the case of 3D model with low excitation frequency is very close to those of dry cylinder. This could be due to zero value of M_{s2} for all modes in the case of low frequency excitation. On the other hand, the results for 3D model with high frequency excitation tend to those of 2D model. However, note that there are appreciable differences in the estimations of the two models for maximum displacement.

TABLE 1. Parameters used in the analyses

Parameter	Value
E (N/m ²)	2.69×10^{10}
h_1, h (m)	100
R (m)	5
t (m)	0.8

TABLE 2. Seismic data used in this study

Input ground motion	Duration (s)	PGA (g)	Epicentral distance (km)
Kobe (1995)	40	0.4862	8.7



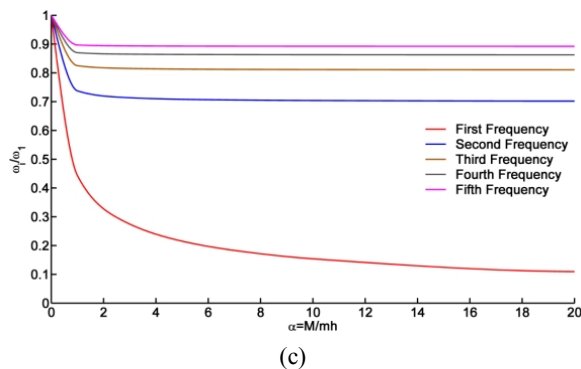


Figure 8. Variations of natural frequencies with change in lumped mass ratio, a) 3D fluid field with high frequency excitation, b) 3D fluid field with low frequency excitation and c) 2D fluid field.

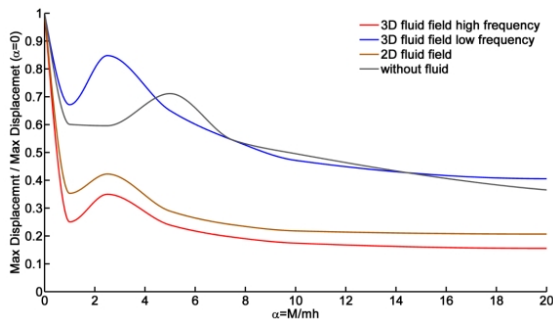


Figure 9. Variations of maximum displacement with change in mass ratio.

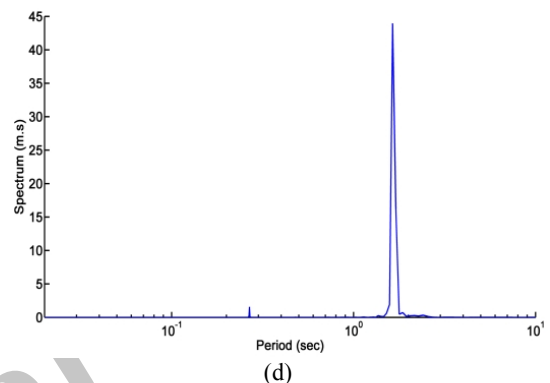
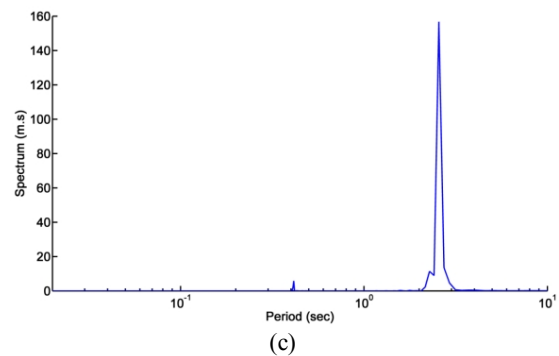
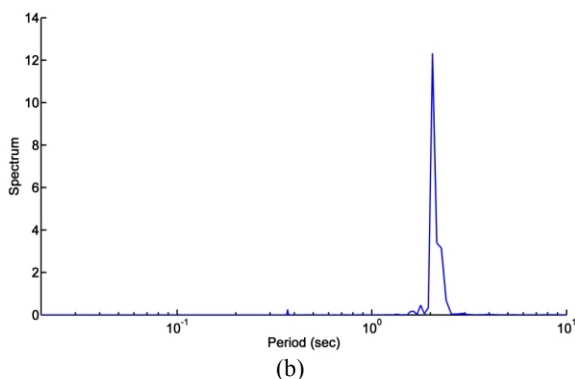
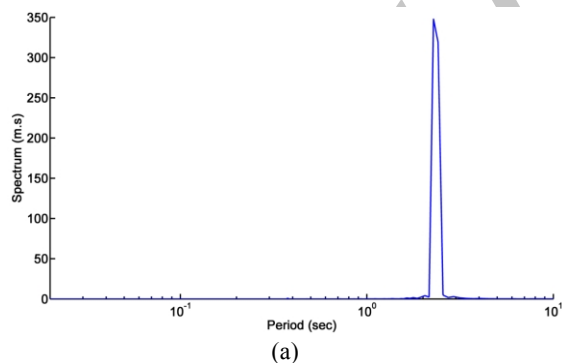


Figure 10. Fourier decomposition of response for different models, a) 3D model with high frequency boundary condition, b) 3D model with low frequency boundary condition, c) 2D model and d) response without fluid.

The result also indicates that in the case of excitation rich in low frequencies, the evaluated maximum displacement employing 2D model will not be on the safe side.

Shown in Figure 10 is the Fourier decomposition of the response for mass ratio of one. As could be seen in all models main contribution comes from the first mode of response and the estimation of different fluid models from this frequency is essentially the same. This also shows that commonly adopted pushover analysis proportional to the first mode of response will give good approximation of actual response.

5. CONCLUSIONS

Response of vertical circular cylinder with a lumped mass at its top and surrounding fluid under ground motion has been investigated. Fluid force along the cylinder body is evaluated employing different approximations for fluid field. These include two dimensional fluid field and also three dimensional fluid field with different assumptions regarding free surface boundary conditions. Deriving the response for 3D models, the evolution of fluid force along the cylinder

body for different excitation frequencies is evaluated. It is shown that for low frequency excitation, the lateral force along the cylinder body comes only from the inertia of the cylinder body and there is no contribution from the surrounding fluid. The results also show that different approximations of the fluid field could have large impact on the value of calculated maximum displacement and in all models the main contribution comes from the first mode.

6. REFERENCES

1. Yeung, R.W., "Added mass and damping of a vertical cylinder in finite-depth waters", *Applied Ocean Research*, Vol. 3, No. 3, (1981), 119-133.
2. Rahman, M. and Bhatta, D., "Evaluation of added mass and damping coefficient of an oscillating circular cylinder", *Applied Mathematical Modelling*, Vol. 17, No. 2, (1993), 70-79.
3. Williams, A.N., "Earthquake response of submerged circular cylinder", *Ocean Engineering*, Vol. 13, No. 6, (1986), 569-585.
4. Tung, C.C., "Hydrodynamic forces on submerged vertical circular cylindrical tanks under ground excitation", *Applied Ocean Research*, Vol. 1, No. 2, (1979), 75-78.
5. Maheri, M. and Severn, R., "Experimental added-mass in modal vibration of cylindrical structures", *Engineering Structures*, Vol. 14, No. 3, (1992), 163-175.
6. Han, R.P., "A simple and accurate added mass model for hydrodynamic fluid—structure interaction analysis", *Journal of the Franklin Institute*, Vol. 333, No. 6, (1996), 929-945.
7. Hsi-The, C., "Earthquake response of circular column submerged in water partially", *Applied Mathematics and Mechanics*, English Edition, Vol. 4, No. 6, (1983), 955-959.
8. Shahmardani, M., Mirzapour, J., Gheyaratmand, C. and Tariverdilo, S., "Moving load analysis of submerged floating tunnels", *International Journal of Engineering*, Vol. 25, No. 1, (2012), 17-24.
9. Anagnostopoulos, S.A., "Dynamic response of offshore platforms to extreme waves including fluid-structure interaction", *Engineering Structures*, Vol. 4, No. 3, (1982), 179-185.
10. Lee, S., Liaw, C. and Tung, C., "Earthquake response of sea-based storage tanks", *Applied Ocean Research*, Vol. 5, No. 3, (1983), 150-157.
11. Bhatta, D. and Rahman, M., "On scattering and radiation problem for a cylinder in water of finite depth", *International Journal of Engineering Science*, Vol. 41, No. 9, (2003), 931-967.
12. Wu, J.-S. and Chen, C.-T., "An exact solution for the natural frequencies and mode shapes of an immersed elastically restrained wedge beam carrying an eccentric tip mass with mass moment of inertia", *Journal of Sound and Vibration*, Vol. 286, No. 3, (2005), 549-568.
13. Öz, H., "Natural frequencies of an immersed beam carrying a tip mass with rotatory inertia", *Journal of Sound and Vibration*, Vol. 266, No. 5, (2003), 1099-1108.
14. Naghipour, M., "Large scale experiments data analysis for estimation of hydrodynamic force coefficients part 1: Time domain analysis", *International Journal of Engineering*, Vol. 14, No. 4, (2001), 323-331.
15. Esper, P., "Numerical modeling of the seismic performance of offshore structures using ANSYS / LS-DYNA", in ANSYS International Conference. (2004).
16. Amundsen, M., "Dynamic analysis of offshore concrete structures subjected to earthquake", in ANSYS International Conference (2012).
17. Tabeshpour, M., Golafshani, A. and Seif, M., "The effect of added mass fluctuation on heave vibration of tlp", *International Journal of Engineering-Materials and Energy Research Center*, Vol. 18, No. 3, (2005), 219-228.
18. Williams, A. and Moubayed, W., "Earthquake-induced hydrodynamic pressures on submerged cylindrical storage tanks", *Ocean Engineering*, Vol. 17, No. 3, (1990), 181-199.
19. To, C., "Vibration of a cantilever beam with a base excitation and tip mass", *Journal of Sound and Vibration*, Vol. 83, No. 4, (1982), 445-460.

Dynamic Response of Submerged Vertical Cylinder with Lumped Mass under Seismic Excitation

M. Shahmardani^a, J. Mirzapour^a, S. Tariverdilo^b

^aDepartment of Civil and Environmental Engineering, Politecnico di Milano, Milan, Italy

^bDepartment of Civil Engineering, Urmia University, Urmia, Iran

PAPER INFO

چکیده

Paper history:

Received 10 January 2014

Received in revised form 15 June 2014

Accepted 26 June 2014

Keywords:

Vertical Circular Cylinder,

Seismic Excitation

Lumped Mass

Added Mass

یک روش تحلیلی برای ارزیابی پاسخ سازه‌های دریایی تحت اثر بار زلزله ارائه شده است. این مقاله اثرات مدل‌های مختلف میدان سیال و جرم تجهیزات در بالای سازه دریایی را که بصورت جرم متمرکز مدل شده را بر روی پاسخ سازه دریایی ارزیابی می‌کند. مدل دو و سه بعدی میدان سیال بسط داده شده است. در مدل‌های سه بعدی تقریب‌های مختلف با توجه به شرایط مرزی سطح آزاد در ارتباط با تحریک فرکانس بالا و پایین اتخاذ شده است. سپس تغییرات پاسخ سازه همراه با تغییر در مقدار جرم متمرکز محاسبه شده است. در نهایت اثرات مدل‌های مختلف به مقدار حداکثر جابجایی برای زمین‌لرزه کوبه ارزیابی شده است. نشان داده شده است که تقریب‌های مختلف در رابطه با میدان سیال تا حد زیادی می‌تواند مقدار حداکثر جابجایی با مدل‌های ارزیابی شده را تغییر دهد.

doi: 10.5829/idosi.ije.2014.27.10a.08